# Vector meson production in $pA$ and $\pi A$ collisions

HADES collaboration

Darmstadt 3.9. 2006

The HADES collaboration

# 1 Introduction

The modification of hadrons in a strongly interacting environment is studied to obtain information on the restoration of the spontaneously broken chiral symmetry at finite temperatures and densities. The order parameter of the chiral symmetry breaking, the chiral condensate $< \bar{q}q >$, has a non-vanishing expectation value in vacuum and is expected to drop by $\approx 30\%$ already at normal nuclear matter density. Although hadron masses are not directly linked to the chiral quark condensate, which is not an observable, QCD sum rules relate the integral over hadronic spectral functions to the non-perturbative quark and gluon condensates.

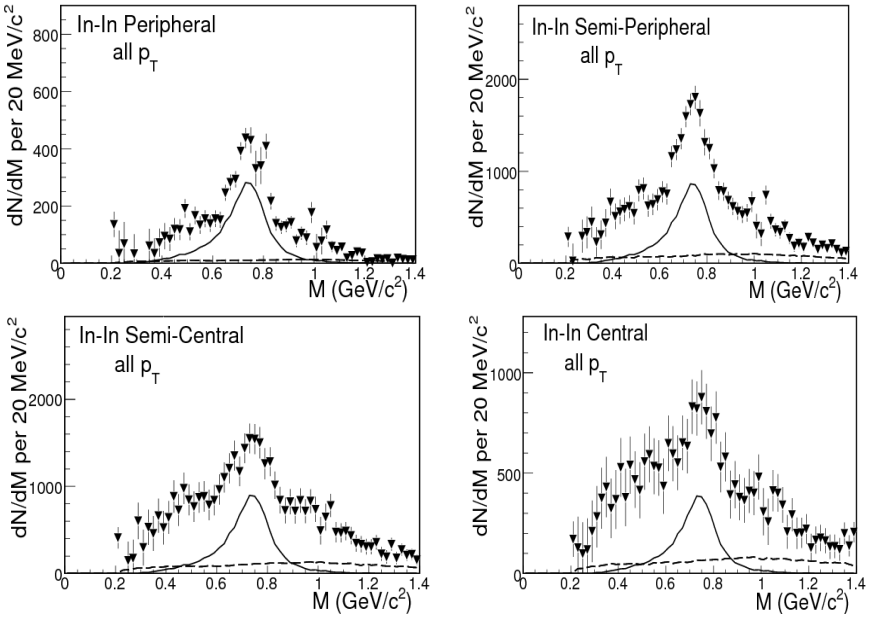


Figure 1: $\rho$ mass distribution, reconstructed from $\mu^+\mu^-$ pairs for different centralities in In+In collisions at 160 AGeV [8].

Predictions of dropping hadron masses in the nuclear medium driven by changes in the chiral quark condensate [1, 2] have triggered widespread experimental and theoretical activities: a lowering of $\rho$ and $\omega$ masses by 15% is expected at normal nuclear matter density [3]. Predictions of dropping hadron masses in the nuclear medium driven by changes. In addition, a broadening of the spectral function to about 70 MeV at normal nuclear matter density is predicted by Klingl et al. [4]. Structures in hadronic spectral functions and a spreading of the strength [5] may arise from a coupling of mesons to nucleon resonances. QCD sum rules calculations claim a sensitivity of the $\omega$ meson mass on the density dependence of 4-quark condensates [6]. This variation in theoretical predictions demonstrates the need for an experimental clarification.

Experimentally, the cleanest approach to study possible in-medium modifications of vector mesons is dilepton spectroscopy, exploiting the decays $\rho, \omega, \phi \rightarrow e^+e^-$. The in-medium mass of the vector meson is reconstructed from the 4-momenta $p_1$ and $p_2$ of the leptons according to

$$m(\rho, T, \vec{p}) = \sqrt{(p_1 + p_2)^2} \tag{1}$$

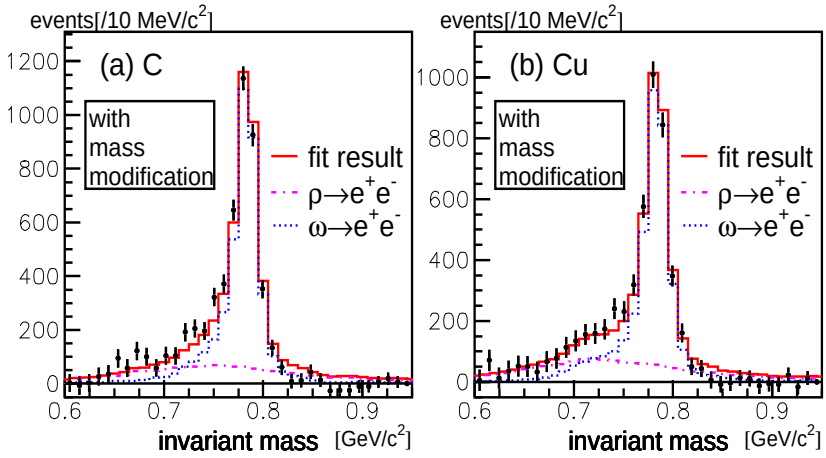


Figure 2: Dielectron invariant mass spectrum in the $\rho - \omega$ region from p C (left) and p Cu (right) collisions. Data were taken at KEK with a 12 GeV proton beam[9].

and depends on the nuclear density $\rho$, temperature T and 3-momentum $\vec{p}$ of the meson. The advantage of the dilepton channel is that leptons do not undergo strong interactions, thereby avoiding any distortion of the invariant mass by final state interactions. The small branching ratio of the order of $10^{-4} - 10^{-5}$ - on the other hand - is a major experimental challenge.

First indications for medium modifications of vector mesons in ultra-relativistic heavy ion collisions were reported by NA45 [7]. The observed enhancement in dilepton yields compared to standard hadronic cocktail expectations is consistent with a shift in spectral strength of the $\rho$ meson towards smaller invariant masses. More recently, the NA60 collaboration has obtained dimuon spectra in In on In collisions with unprecedented statistics and mass resolution [8] which indicate a strong broadening of the $\rho$ meson but no mass shift with increasing centrality of the reaction (Fig. 1).

Heavy-ion experiments necessarily provide signals which are integrated over the space-time evolution of the collision involving significantly changing densities and temperatures. In contrast, elementary photon or hadron induced reactions allow an access to medium modifications under better controlled conditions. Experiments with proton and photon beams have recently been performed at KEK and JLab. The KEK group reports a drop of the $\rho$ mass by 10% at normal nuclear matter density but no in-medium broadening, as shown in Fig. 2 [9]. On the other hand, preliminary results from the CLAS experiment indicate no mass shift of the $\rho$ meson but some moderate in-medium broadening [10]. This confusing situation calls for additional experiments using different elementary reactions and detector systems. It should be noted that both experiments are only sensitive to rather high recoil momenta of the vector mesons ($> 1$ GeV/c) because of the high incident energies and detection thresholds.

In-medium modifications of the $\omega$ meson were reported by the CBELSA/TAPS collaboration, studying the $\omega \rightarrow \pi^0\gamma$ channel [11]. This channel is adventageous due to the high branching ratio of 8% [13] and the fact that a possible in-medium modification of the $\rho$ meson can not distort the $\omega$ signal because of the low branching ratio of $7{\cdot}10^{-4}$ for the $\rho \rightarrow \pi^0\gamma$ channel. The disadvantage of the $\pi^0\gamma$ decay mode is a possible final state interaction of the $\pi^0$ meson which can, however, be suppressed by suitable cuts on the kinetic energy of the pion

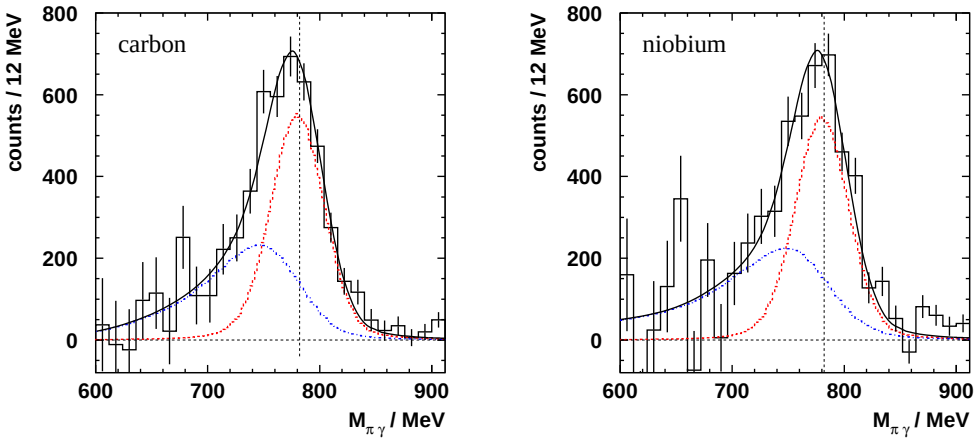


Figure 3: Decomposition of the $\omega$ signal (from the $\pi^0\gamma$ decay channel) into a contribution of in-vacuum decays (red curves) and an in-medium ($\rho \geq 0.1\rho_0$) contribution (blue curves). The data on Carbon (left figure) and on Niobium (right figure) are from CBELSA/TAPS [14].

[12]. A comparison to BUU simulations [13] shows that the observed signal (see Fig. 3) is consistent with a dropping $\omega$ mass according to

$$m_\omega = m_0 \cdot (1 - 0.16\rho/\rho_0) \tag{2}$$

Furthermore a broadening of the $\omega$ meson to about 90 MeV at normal nuclear matter density is deduced from the dependence of the $\omega$ meson yield on the atomic mass number, analyzing the transparency ratio [14] in an analoguous way as for the $\Phi$ meson [15].

$$T = \frac{\sigma_{\gamma A \to \omega X}}{A \cdot \sigma_{\gamma N \to \omega X}} \tag{3}$$

The CBELSA/TAPS experiment suffers from the limited invariant mass resolution of 3%. This can be improved by a factor ≈2 if the design momentum resolution of HADES is achieved. Although the authors of [11] believe to have the systematic errors associated with the $\pi^0$ rescattering under control, it is important to verify their result in a different decay channel. In addition, the above mentioned discrepancy between the KEK and JLab experiments [9, 10] calls for a new attempt to determine the in-medium properties of the $\rho$ and $\omega$ meson.

The proposed experiment at HADES using proton and pion beams has the following advantages compared to the above experiments: it avoids the integration over the space-time evolution of the reaction (in comparison to the NA60 experiment) and it is sensitive to low recoil momenta of the vector mesons ($p \leq 1GeV/c$), allowing a simultaneous study of medium modifications of both, $\rho$ and $\omega$ mesons, in contrast to the KEK and Jlab measurements. In comparison to the CBELSA/TAPS experiment a better invariant mass resolution is expected and posssible systematic errors associated with the $\pi_0\gamma$ exit channel can be avoided. The proposed experiment is described in the following sections.

## 2 $\rho/\omega$ production in $pA$ and $\pi$A collisions

The Hadron String Dynamics (HSD) model has been used to calculate vector meson production in $pA$ and $\pi A$ reactions. HSD combines a parametrization of experimental cross sections for meson production in $NN$ and $\pi N$ reactions with One Boson Exchange (OBE) and Lund String

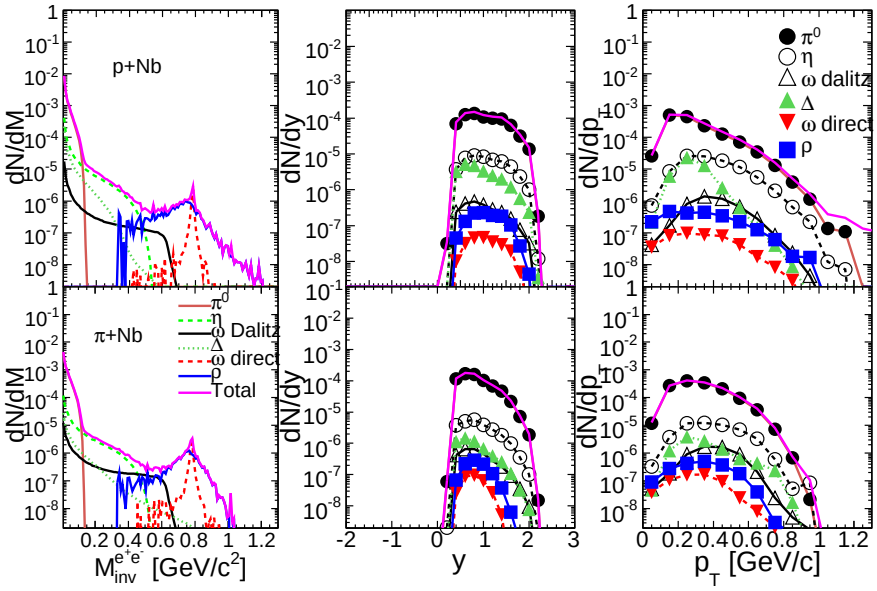


Figure 4: Dielectron invariant mass, rapidity and transverse momentum spectra for $pNb$ at 3.5 GeV (upper panels) and $\pi Nb$ at 1.17 GeV (lower panels) after HADES acceptance and reconstruction efficiency filter.

(LSM) models and a covariant hadronic transport which takes the dynamics of vector meson production and propagation in the nucleus into account [16]. One should note, however, that inclusive vector meson production in $pp$ and $\pi N$ reactions at $\sqrt{S} - \sqrt{S_{thres}} < 1$ GeV is only partially known. In particular, inclusive $\omega$ production in $pp$ collisions is only accessible via OBE and LSM calculations. The goal of the approved pp experiment at 3.5 GeV is to provide data in this energy range.

In the following we have studied the $\omega$ and $\rho$ properties using proton and pion beams at different incident energies with different target nuclei. For event by event simulations needed for background or trigger studies, discussed in the next chapter, we have used the PLUTO generator. In order to get the actual number of $\omega$'s and $\rho$'s to be detected in HADES we apply the full HADES geometrical acceptance and reconstruction efficiency filter. The filters were determined from Monte-Carlo simulations using electron tracks with uniform momentum and isotropic angular distributions. All events were digitized with a realistic detector response function and processed through the same analysis chain as the measured data. The single-electron acceptance and reconstruction efficiencies, $AE_{\pm}(p, \theta, \phi)$, were calculated as a function of charge ($\pm$), momentum ($p$), polar ($\theta$) and azimuthal ($\phi$) angles and reflect the fraction of all electron emitted in the full solid angle which were identified and reconstructed in the HADES coverage. The pair acceptance has been obtained as the product of corresponding single-electron acceptances $AE_+$ and $AE_-$. The results after filtering are shown in Figure

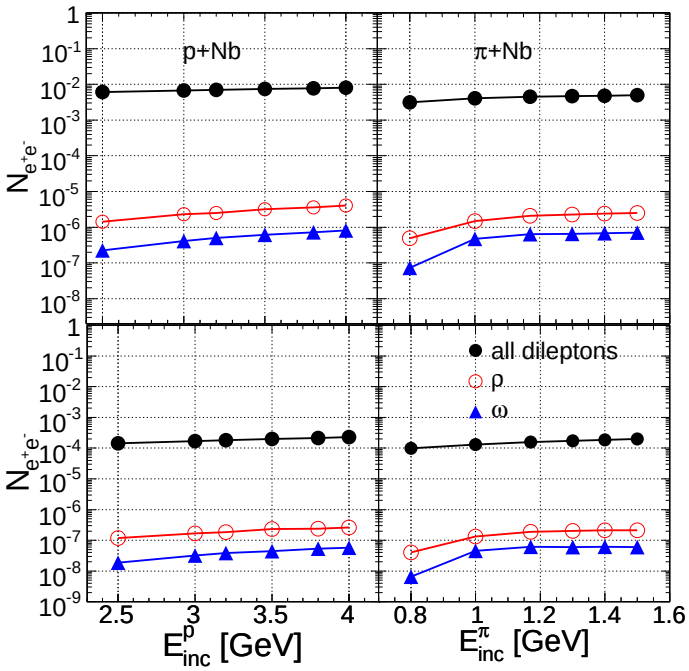


Figure 5: Total integrated dielectron production probability as a function of incident energy for the $pNb$ case (left) and for the $\pi Nb$ case (right). Upper panels are obtained from HSD simulations without any acceptance cut. Lower panels are HSD results filtered by the HADES acceptance and efficiency. In the $\rho$ and $\omega$ cases, the HADES filter leads to a reduction by a factor 10.

4. The $\rho$ and $\omega$ distributions fit nicely within the HADES acceptance. Neither acceptance nor efficiency produces significant changes of shapes of the primary distributions. Whereas the collisional broadening has been taken into account in the propagation of vector mesons in the nuclear medium, the spectral functions used at the decay point are the free ones. Therefore vector mesons show up with the free width in the figures.

The integrated dielectron production probability for all sources and the direct decays of vector mesons as a function of the incident beam energy for the $Nb$ target are shown for the proton and pion projectiles in the upper panels of Figure 5. The dielectron probabilities for both pion and proton beams are of the same order. The total $\omega$ and $\rho$ yields increases for $p$-induced reactions as we go up in incident energy, but it remains about the same for $\pi$-induced reactions except for the lowest energy (0.8 GeV). The lower panels of Figure 5 show the total integrated dielectron detection probability both for proton and pion induced reactions after using the filter. After filtering, the integrated $\omega$ and $\rho$ yields decreases an order of magnitude for all incident energies. This reduction of the yields is due to geometrical acceptance ($\sim$0.35) and reconstruction efficiency ($\sim$0.25), resulting in a reduction factor for accepted $\rho$ and $\omega$ of about 0.1.

Since the $\omega$ and $\rho$ change their properties inside the nuclear matter it is of interest to study how many of them decay inside the nucleus. This is illustrated in Fig. 6 where the spatial distribution of production and decay points of $\omega$ mesons in both, $\pi$ and $p$ induced reactions are plotted in comparison to the contours of a $Nb$ nucleus. Decays at densities larger than 10% of normal nuclear matter density are considered in-medium, decays. The left panel of Fig. 9 shows the cross section of $\omega$'s and $\rho$'s which decay inside the nucleus as a function of the incident

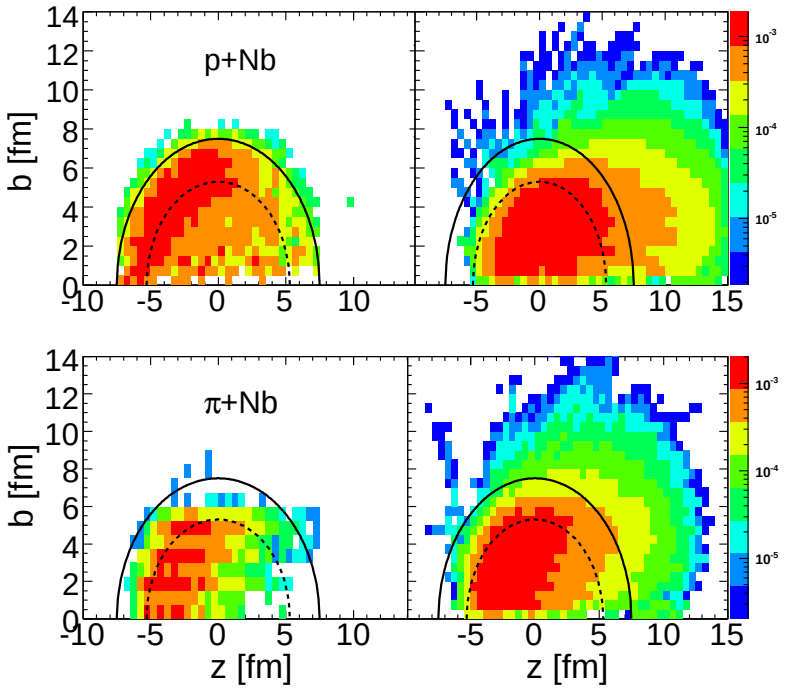


Figure 6: Radial (b=$\sqrt{x^2+y^2}$) vs. longitudinal coordinate (z) of the $\omega$ production and decay (left and right panels, respectively). The upper panels show the results for $pNb$ reactions at 3.5 GeV and lower ones for $\pi Nb$ reactions at 1.17 GeV. The full and dashed half-circles correspond to 10% and 90% of the nuclear density, respectively.

energy for $pA$ and $\pi A$ reactions. At the respective energies of 1.3 GeV and 3.5 GeV these cross sections are comparable. The right panel gives the percentage of inside decays of $\omega$'s and $\rho$'s as a function of incident energy.

For the $\pi$-induced reaction the fraction of inside decays of the $\omega$ is higher as compared to the $p$-induced case since the momentum of the produced $\omega$'s are lower on average because of the lower energy above threshold. At the incident $\pi$ energy of 1.17 GeV about 65% of $\omega$'s decay inside the nucleus. The percentage of inside decay of the $\omega$'s does not change much as we increase the energy. At the incident $p$ energy of 3.5 GeV about 44% of the $\omega$'s decay inside the nucleus. On the other hand most of the $\rho$ mesons decay inside the nucleus for both reactions. For the $\pi$-induced case, about 90% of the $\rho$'s decay inside the nucleus and for the $p$-induced case it is about $75-80$%. This is due to the shorter life time of the $\rho$ (for free $\rho$ it is $\sim$1.3 fm/c) compared to the free life time of the $\omega$ ($\sim$23 fm/c). This difference is, however, partially compensated by the strong in-medium broadening of the $\omega$ meson.

Since in-medium modifications of the vector meson spectral functions depend on the meson momentum, it is interesting to compare these distributions for the proton and pion case. The momentum distributions for $\rho$'s and $\omega$'s, which decay inside and outside of the $Nb$ nucleus, are shown in Figure 8. As mentioned above, the average vector meson momentum is lower in case of the pion induced reactions. The dielectron cross sections of $\omega$'s and $\rho$'s for a proton beam of 3.5 GeV as a function of different targets is shown in the left panel of Figure 9. The right panel shows the percentage of $\omega$ and $\rho$ decays inside the nucleus as a function of mass of the target without any momentum cut. For the targets of higher masses as compared to $Nb$,

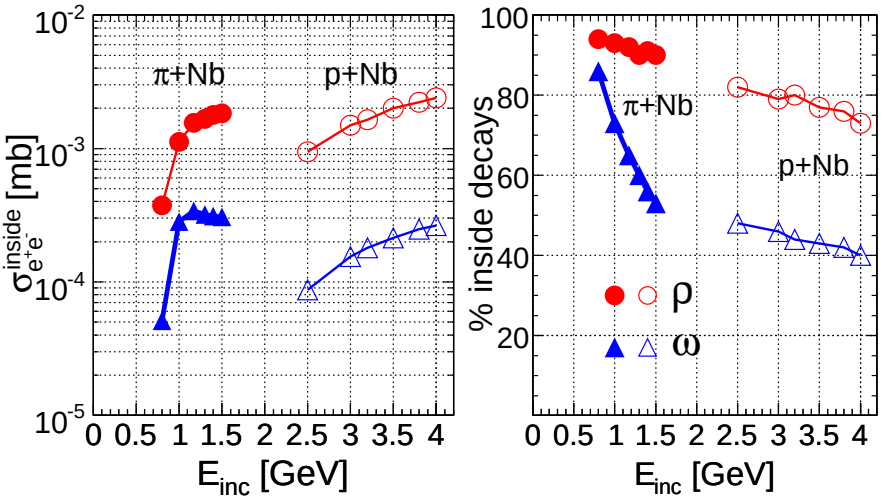


Figure 7: Cross section for $\omega$ and $\rho$ decays inside the $Nb$ nucleus (left panel) and the fraction of $\omega$ and $\rho$ decays inside the $Nb$ nucleus (right panel) as function of the incident energy for $\pi$-induced (closed symbols) and $p$-induced (open symbols) reactions.

the dielectron cross sections as well as the percentage of inside decays only slightly increases. Comparing $Nb$ and $Pb$ target, there is a gain of about 10% and 20% in inside decays of $\rho$ and $\omega$, respectively, while the gamma conversion probability increases by at least factor $2-3$ (see next chapter). The choice of a Niobium target was also made by the CBELSA/TAPS and JLAB experiments and its realization is technically easy. Therefore we have considered $Nb$ target as the better choice for our experiment.

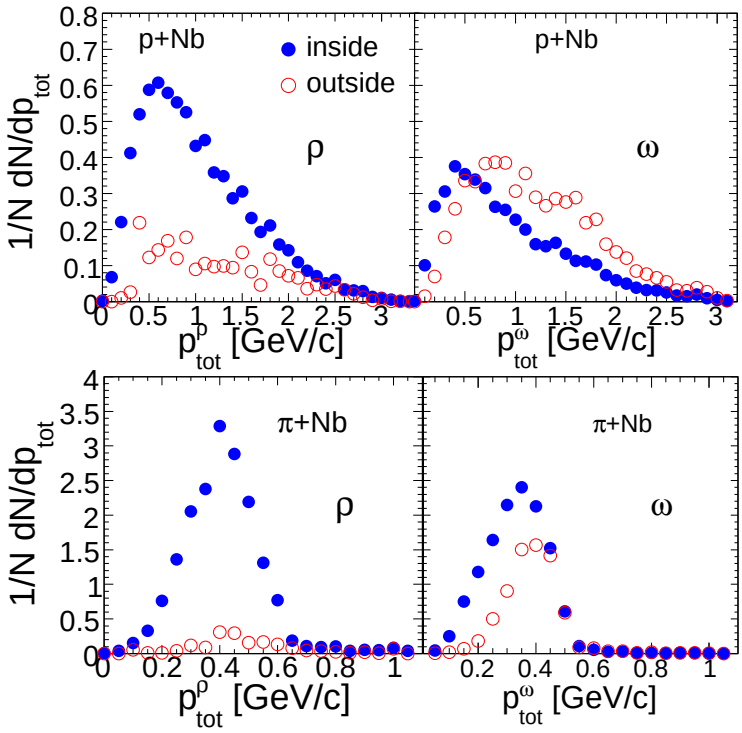


Figure 8: Laboratory momentum distributions for inside and outside decay of $\rho$'s (left) and $\omega$'s (right) for $pNb$ reactions at 3.5 GeV incident energy (upper panels) and for $\pi Nb$ reactions at 1.17 GeV (lower panels).

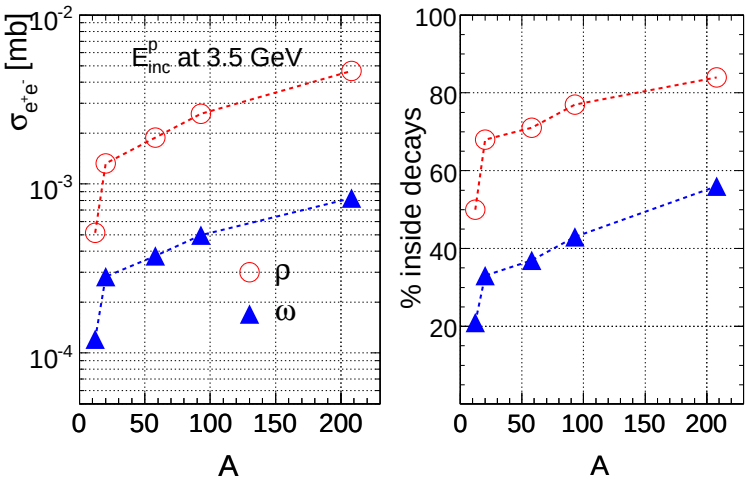


Figure 9: Dielectron cross section (left panel) and fraction of decay (right panel) of $\rho$'s and $\omega$'s inside the nucleus for different target nuclei at an incident proton energy of 3.5 GeV.

# 3 Background and signal reconstruction

Combinatorial Background (CB) is a major background source for this experiment and therefore has to be carefully studied. To do so we have used the PLUTO event generator based on hadron multiplicities derived from the HSD transport calculation [18] and a fast analysis programme. The analysis programme takes into account the HADES geometrical acceptance and the electron reconstruction efficiencies via dedicated filters described below. Furthermore, it generates conversion pairs from photons originating mainly from $\pi^0$ decays. The latter are stored in the PLUTO output. Photon conversion is treated by a dedicated function generating electron pairs based on known pair creation cross sections and taking into account the material budget of the targets and the RICH radiator. No conversion outside the target and radiator was considered since conversion pairs which do not produce Cherenkov rings in the RICH detector are not recognized as electron tracks in HADES. In the next step, the simulated events were filtered through the HADES geometrical acceptance and the known reconstruction efficiencies were applied. Furthermore, a minimum pair opening angle of $9^0$ was required, also including incompletely reconstructed tracks (i.e. in the inner MDC chambers, only), to reduce combinatorial background originating from conversion and $\pi^0$ Dalitz decay. This fast simulation was tested and proven to be reliable in the analysis of the C+C run at 2 $A$GeV.

In the simulations of $pA$ reactions we have assumed a target consisting of two sections of ${}^{93}_{41}Nb$ (production) interleaved by one ${}^{9}_{4}Be$ (reference) section. The distance between the $Nb$ and $Be$ sections amounts to 12 mm to allow separation of three production vertices. Each $Nb$ section consists of two discs of $d = 3$ mm diameter and $t_a = 1.0$ mm thickness ($\approx 0.1$ $X_0$) displaced by 5 mm to minimize conversion in the target. The $Be$ section consists of two discs with the same diameter and thickness of $t_b = 4.0$ mm each, displaced by 5 mm. The total target thickness in terms of interaction probability amounts to 4% with 2% for $Be$ and 2% for $Nb$, respectively. The ${}^{9}_{4}Be$ target section is necessary to control systematic effects related to the $e^+e^-$ invariant mass reconstruction. Furthermore, it provides a reference measurement of the vector meson line shape for a light nucleus. The selection of ${}^{9}_{4}Be$ is motivated by a low conversion probability (see below) and by practical reasons (target machining). One should also note that the proton/neutron ratio is the same as for ${}^{93}_{41}Nb$. The target thickness has been calculated according to the formula:

$$t = \frac{I_0 A}{\rho \sigma N_A}$$

where $N_A = 6.023 \cdot 10^{23}$ is the Avogadro number, $\rho$ is the target density, $\sigma$ is the the total geometrical cross section : $\sigma = \pi r_0^2 A^{2/3}$ ( $r_0 = 1.21 \cdot 10^{-13}$ cm) and $I_0$ is the reaction probability. Table 1 shows the relevant target parameters.

| **Target** | A | Z | $\rho$ | $\sigma$ [b] | t [mm] |
|---|---|---|---|---|---|
| Be | 9 | 4 | 1.848 | 0.2 | 8.0 |
| Nb | 93 | 41 | 8.57 | 0.92 | 4.0 |
| Pb | 207 | 82 | 11.35 | 1.55 | 3.9 |

Table 1: Target parameters for an interaction probability of $I_0 = 2\%$

The particle yield distributions used in the PLUTO generator were taken from the HSD code and are shown in table 2. For particle emission a thermal source with temperature $T = 82$ MeV,

| **Source** | Multiplicity | $BR$ |
|---|---|---|
| $\pi^0 \rightarrow e^+e^-\gamma$ | 0.6 | $1.2 \cdot 10^{-2}$ |
| $\Delta \rightarrow Ne^+e^-$ | 0.9 | $4.4 \cdot 10^{-5}$ |
| $\eta \rightarrow e^+e^-\gamma$ | $3.1 \cdot 10^{-2}$ | $6.0 \cdot 10^{-3}$ |
| $\omega \rightarrow e^+e^-$ | $1.0 \cdot 10^{-2}$ | $7.15 \cdot 10^{-5}$ |
| $\omega \rightarrow \pi^0e^+e^-$ | $1.0 \cdot 10^{-2}$ | $5.9 \cdot 10^{-4}$ |
| $\rho \rightarrow e^+e^-$ | $7.12 \cdot 10^{-2}$ | $4.48 \cdot 10^{-5}$ |
| $\phi \rightarrow e^+e^-$ | $4.4 \cdot 10^{-4}$ | $3.0 \cdot 10^{-4}$ |
| $p$ | 2.03 | |
| $\pi^{+(-)}$ | 0.6 | |

Table 2: Multiplicity of hadrons with dielectron decay branches (upper part) and respective branching ratios assumed in a simulation of the $p + A$ reaction at a beam kinetic energy of 3.5 GeV. Branching ratios are taken from PDG [19] and multiplicities from HSD calculations. Multiplicities of protons and charged pions are shown in the lower part

as obtained from a fit to corresponding $m_T$ distributions, was assumed. Furthermore, in order to reduce computing time, dielectron decay branches were enhanced and respective weights stored in the simulated event structure, which contained the four momentum components of electrons, positrons and photons from hadron decay. In addition to the leptonic final state, charged pions and protons were also included to simulate the trigger conditions. The results of the simulation are presented in Figure 10. The left panel shows the mass distribution of the signal, its decomposition into the most important sources and the combinatorial background. As one can see, the signal to CB ratio in the interesting mass region ($M > 400$ MeV/c$^2$ increases from 1 at $M \sim 400$ MeV/c$^2$) to $> 10$ near the vector meson mass poles. For comparison, we show in the right panel the respective distributions for reactions of protons with a 2% $Pb$. The significantly larger CB is due to photon conversion in the target material. On the other hand, as we have shown in the previous chapter, the vector meson yield increases only by 20% when going from a $Nb$ to a $Pb$ target. Consequently, the spectral function of vector mesons can be measured with a better signal to background ratio if a medium heavy target is used. The prominent structure appearing in the CB distribution around $M_{e+e-} \sim 100$ MeV/c$^2$ originates from simultaneous conversion of both photons from the $\pi^0$ decay. Please note the different $\rho$ meson shape in PLUTO simulation as compared to the HSD shown in the previous section. It results from the thermalization assumption which leads to a enhanced population of mesons in the low-mass tail of the spectral function, extending down to the kinematic threshold $M = 2 * M_e$.

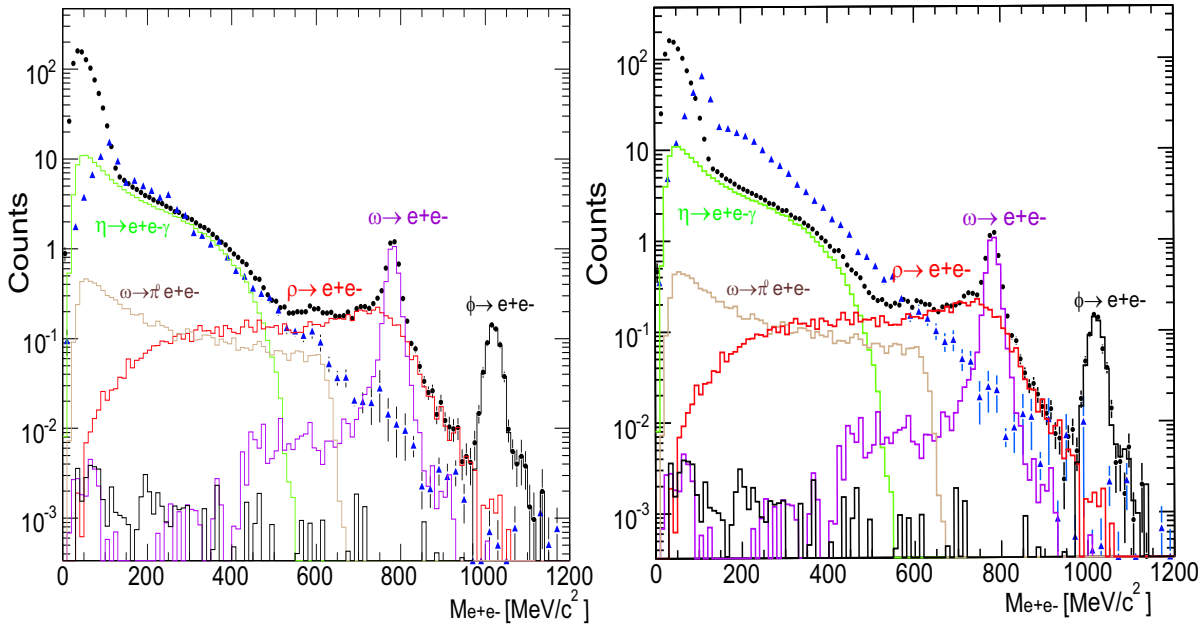


Figure 10: Simulated $e^+e^-$ invariant mass distributions for signal (black dots) and combinatorial background (blue triangles) for $55 \cdot 10^6$ $p + Nb$ (left) and $p + Pb$ (right) collisions at 3.5 GeV. Most important cocktail components are shown separately. The CB is due to conversion of photons from $\pi^0$ and $\eta$ decays.

# 4 Summary and shift request

Table 3 presents count rate estimates for vector meson detection in HADES for the $p + Nb$ and $\pi + Nb$ case. For proton induced reactions the beam intensity is limited by the maximally acceptable LVL1 trigger rate of 20 kHz. The LVL1 trigger condition requires at least 2 charged particles inside the HADES acceptance and is realized by a fast multiplicity measurement in the META and the inner MDC chambers. According to simulation, this condition reduces the

| | $p + Nb$ 3.5 GeV | $p + Nb$ 4.5 GeV | $\pi + Nb$ 1.17 GeV |
|---|---|---|---|
| $Beam[1/s]$ | $1.0 \cdot 10^6$ | $1.0 \cdot 10^6$ | $1.0 \cdot 10^6$ |
| $L$ | $5.5 \cdot 10^{27}$ | $5.5 \cdot 10^{27}$ | $5.5 \cdot 10^{27}$ |
| $P(\omega \rightarrow e^+e^-)$ | $6.85 \cdot 10^{-7}$ | $9.19 \cdot 10^{-7}$ | $6.51 \cdot 10^{-7}$ |
| $Acc \cdot Eff$ | 0.08 | 0.08 | 0.1 |
| $Rate[day]$ | 24.0 | 32 | 28 |
| $P(\rho \rightarrow e^+e^-)$ | $3.73 \cdot 10^{-6}$ | $4.86 \cdot 10^{-6}$ | $2.17 \cdot 10^{-6}$ |
| $Acc \cdot Eff$ | 0.08 | 0.08 | 0.1 |
| $Rate[day]$ | 130 | 170 | 95 |

Table 3: Upper part: Beam intensity and averaged luminosity for $pNb$ and $\pi Nb$ experiments. Lower part: Dielectron rates from the vector meson decays.

primary trigger rate as given by the total reaction cross section by a factor of 2. Hence, a beam of 1 million protons per second on a 4% target will lead to a LVL1 trigger rate of 20 kHz. Moreover, we account for an average DAQ dead time of 50% and an effective machine duty factor of 50%, to compute the mean luminosity, which turns out to be 4 times smaller then the peak rate. The expected mean luminosities (shown in Table 3) are then calculated from:

$$L = \rho \cdot t \cdot I_{beam} \cdot N_A/A \cdot 0.25$$

Here $\rho$,$t$,$A$ are target parameters given in Table 1 and $I_{beam}$ is the beam intensity in particles per second. The rate per day is then given by

$$Rate = L \cdot P(\omega \rightarrow e^+e^-) \cdot AE \cdot N_s \cdot \sigma$$

where L is the luminosity, P the probability for a vector meson to decay within the HADES acceptance, $AE$ is the $Acceptance \cdot Efficiency$ factor, $N_s$ the number of seconds per day and $\sigma$ the total reaction cross section.

For the pion beam we also assumed a maximal beam intensity of $10^6$ $\pi^-$. One should note, however, that this intensity is by a factor 2 larger than the one achieved under best conditions in a machine test run in 2005 with $6.5 \cdot 10^{10}$ $^{14}N$ ions (50% of space charge limit in SIS). Moreover, pion beam tracking with in-beam hodoscopes and the beam halo further reduces the effective luminosity. We therefore conclude that the statistics with a $\pi$ beam would not be enough. This is the reason why we propose in a first step to run the experiment with a proton beam. Moreover, the HADES running conditions with a proton beam are quite well under control, as demonstrated in recent experiments. Whereas the pion case seems more appropriate for producing low momentum vector mesons, thereby enhancing the inside decay probability and offering the possibility to explore the momentum dependence of the in-medium vector meson

spectral function, it suffers today from several drawbacks which have to be clarified first. The installation and respective tests with the new additional quadrupole in front of the HADES detector are also mandatory steps before going to a production run. Dedicated tests should then happen first at the machine level and for establishing the best running conditions (trigger, halo, in-beam hodoscope). We request for this program a **total commissioning $\pi$ beam time of 20 shifts**. The request for the **proton nucleus run** amounts to $(((\frac{1000}{24} \times 1.15) + 7) \times 3 \simeq)$ **165 shifts** and is based on the following arguments: (1) we consider that a statistics of at least 1000 $\omega$ mesons for each target is needed, which results in 42 days. (2) We include 15% to accommodate possible parasitic users. (3) For tuning the beam and the detector parameters and for zero field and other calibration runs we request, based on experiences from previous proton runs, one additional week. The choice of an energy of 3.5 GeV is dictated by the following arguments: (a) The gain in total vector meson rate and inside decays rate is marginal, only 20%, when going from 3.5 GeV to 4.5 GeV. (b) The energy of 3.5 GeV corresponds to the energy where we will run the elementary pp measurements. (c) The invariant mass resolution in the $\omega$ mass region is significantly better at 3.5 GeV, since it scales with lepton mean momenta. (d) The energy of 3.5 GeV will provide a better window for the study of the momentum dependance of the in-medium vector meson spectral function. A similar application for running the experiment with the pion beam will be submitted to a forthcoming PAC meeting.

# References


[1] G.E. Brown and M. Rho, Phys. Rev. Lett. 66 (1991) 2720

[2] T. Hatsuda and S. Lee, Phys. Rev. C46 (1992) R34

[3] K. Saito, K. Tushima, and A.W. Thomas, Phys. Rev. C55 (1997) 2637

[4] F. Klingl, T. Waas, W. Weise, Nucl. Phys. A 650 (1999) 299

[5] M. Lutz et al., Nucl. Phys A 706 (2002) 431

[6] S. Zschoke et al., Phys. Lett. B562 (2003) 57

[7] G. Agakishiev et al.,Phys. Rev. Lett 75(1995) 1272

[8] R. Arnaldi et al., Phys. Rev. Lett. 96 (2006) 162302

[9] Naruki et al., Phys. Rev. Lett. 96 (2006) 092301

[10] R. Nasseripour, private communication, 2006

[11] D. Trnka et al., Phys. Rev. Lett. 94 (2005) 192303

[12] J. Messchendorp et al, Eur. Phys. J. A11 (2001) 95

[13] P. Mühlich, T. Falter, and U., Mosel Eur. Phys. J. A. 20 (2004) 499

[14] D. Trnka, PhD-thesis, University of Giessen, 2006

[15] T. Ishikawa et al., Phys. Lett. B 608 (2005) 215

[16] W. Cassing and E. L. Bratkovskaya, Phys. Rep. 308, 65 (1999).

[17] Landolt-Börnstein, New Series I/12b.

[18] M. Kargalis, GSI report 2000.

[19] Particle Data Group, Phys. Rev. D54 (1996)

[20] HADES collaboration, submitted to Phys. Rev. Lett(2006)

[21] S. Teis et al., Z. Phys. A356 (1997) 421., nucl-th/96090009

[22] C. Fuchs et al., Phys. Rev. C 025202(2003)

[23] B. Spruck et al., GSI annual report 2005